PAPER

Check for updates

An Fe₃O₄ supported *O*-phenylenediamine based tetraaza Schiff base-Cu(ɪɪ) complex as a novel nanomagnetic catalytic system for synthesis of pyrano[2,3-*c*]pyrazoles†

Rehab Tahseen alhayo,[a] Ghufran Sh. Jassim, [iD] [b] Hasanain Amer Naji,[c] A. H. Shather,[d] Israa Habeeb Naser,[e] Luay Ali Khaleel[f] and Haider Abdulkareem Almashhadani [iD] *[g]

In this research, we present a post-synthetic method for synthesizing a novel nanomagnetic Cu(ɪɪ) Schiff base complex and investigate its efficiency in catalytic organic conversion reactions. Various spectroscopic analyses were employed to characterize the physiochemical characteristics of the resulting nanocomposite. The experimental results successfully demonstrate the catalytic application of the prepared Cu-complex in the preparation of pyrano[2,3-*c*]pyrazole heterocycles. This synthesis involved a one-pot three-component condensation reaction, wherein hydrazine hydrate, ethyl acetoacetate, malononitrile, and aromatic aldehydes were combined under reflux conditions using water as the solvent. Notably, the heterogenized complex exhibited exceptional catalytic performance, achieving remarkable conversion rates and selectivity, all accomplished using only 12 mg of the catalyst. Furthermore, thorough stability assessments of this catalyst were conducted through reusability and hot filtration tests, which confirmed its non-leaching properties and demonstrated excellent results over the course of five consecutive runs.

1. Introduction

Pyrano[2,3-*c*]pyrazoles represent a significant group of heterocycles that have attracted significant attention within the realm of medicinal chemistry and drug discovery.[1] The scaffold of these structures consists of a pyrazole ring fused with a pyran ring, forming a fused heterocyclic framework. This unique structural motif provides a versatile platform for molecular modifications and exhibits diverse biological activities, enabling the synthesis of various derivatives with enhanced biological properties.[2]

The pyrano[2,3-*c*]pyrazoles synthesis involves diverse strategies, such as multicomponent reactions, cyclization reactions, or condensation reactions, which allow for the introduction of different functional groups and substitution patterns.[2–5] One commonly employed strategy involves the condensation reaction between pyrazole derivatives and α,β-unsaturated carbonyl compounds, such as α,β-unsaturated ketones or aldehydes, under acidic or basic conditions.[6] Another synthetic approach involves the cyclization of α,β-unsaturated ketones with hydrazine derivatives, followed by oxidative cyclization or ring-closing reactions using suitable reagents or catalysts. On the other hand, multicomponent reactions, such as the one-pot condensation of α,β-unsaturated carbonyl compounds, hydrazine derivatives, and active methylene compounds such as malononitrile, have been employed as the most efficient and simple method for this synthesis.[7] In this regard, several catalytic methods have been employed for these reactions. One notable approach involves the use of Lewis acid catalysts, such as Zn, Fe and Cu complexes, which promote the generation and condensation of pyrazolone and α,β-unsaturated carbonyl intermediates, facilitating the cyclization process and resulting in the selective production of the fused pyrano[2,3-*c*]pyrazole rings at enhanced reaction rates.[8–10] The use of catalytic methods provides several advantages, including increased reaction rates, improved yields, and enhanced control over regioselectivity and stereoselectivity, making them valuable tools in these transformations.

Heterogeneous magnetic catalysts are a promising class of materials in catalysis due to their unique combination of

[a]Al-Farahidi University, College of dentistry, Baghdad, Iraq

[b]Department of Chemistry, College of Science, University of Anbar, Anbar, Iraq

[c]Faculty of Pharmacy, Al-Turath University College, Baghdad, Iraq

[d]Department of Computer Engineering Technology Al Kitab University,Altun Kopru, Kirkuk 00964, Iraq

[e]Medical Laboratories Techniques Department / AL-Mustaqbal University College, 51001 Hillah, Babil, Iraq

[f]Collage of Dentistry, National University of Science and Technology, Dhi Qar, Iraq

[g]Chemistry Department, College of Science, University of Baghdad, Baghdad, Iraq. E-mail: haider.200690@gmail.com; h_r200690@yahoo.com

† Electronic supplementary information (ESI) available. See DOI: https://doi.org/10.1039/d3na00906h

magnetic properties and catalytic functionality.[11–15] These catalysts offer advantages such as enhanced catalyst recovery, recyclability, and improved reaction kinetics.[15–18] Compared to traditional catalysts, heterogeneous magnetic catalysts simplify catalyst recovery, reduce costs, and minimize environmental impact.[19,20] Additionally, their recyclability ensures long-term viability and economic feasibility, making them an attractive option in catalysis applications.[21] The active regions located on the surface of the magnetic core or attached functional coatings enable a wide range of an extensive variety of catalytic reactions.[22]

In this regard; heterogeneous Schiff base catalysts are crucial in organic synthesis, promoting diverse and efficient chemical transformations.[23,24] These catalysts consist of immobilized Schiff base ligands on solid supports, offering advantages such as enhanced catalytic activity, improved selectivity, and recyclability.[25–27] They are compatible with a wide range of substrates, enabling the synthesis of various organic compounds with high yields and purity.[28] The tunable and robust nature of these catalysts allows for the development of new synthetic methods and exploration of complex transformations.[29,30] Overall, heterogeneous Schiff base catalysts play a vital role in advancing organic synthesis, providing efficient and environmentally friendly routes to valuable organic molecules.[31]

Overall, the unique combination of magnetic properties and catalytic efficiency of Schiff base complexes holds great promise for catalysis applications, opening new avenues for efficient and sustainable chemical transformations. Now, in this paper, a Schiff base complex of copper immobilized on magnetic Fe$_3$O$_4$ nanoparticles [Fe$_3$O$_4$@SiO$_2$-Schiff base-Cu$^{(II)}$] was successfully fabricated as a novel and efficient magnetically recoverable nanocatalyst for the multicomponent synthesis of pyrano[2,3-c]pyrazoles.

2. Experimental

2.1. Typical procedure for the synthesis of [Fe$_3$O$_4$@SiO$_2$-Schiff base-Cu$^{(II)}$] complex

In the first step, silica-modified Fe$_3$O$_4$ MNPs were prepared using a previously established procedure.[32] Simultaneously, 2 g of Fe$_3$O$_4$@SiO$_2$ MNPs were dispersed in 100 mL of 95% ethanol, and a 20 mL solution of 0.25 M 3,4-diaminobenzoic acid in ethanol was added to the well-dispersed suspension and then refluxed for 12 hours under N$_2$ atmosphere. Afterward, the resulting Fe$_3$O$_4$@SiO$_2$-diamine powder was magnetically
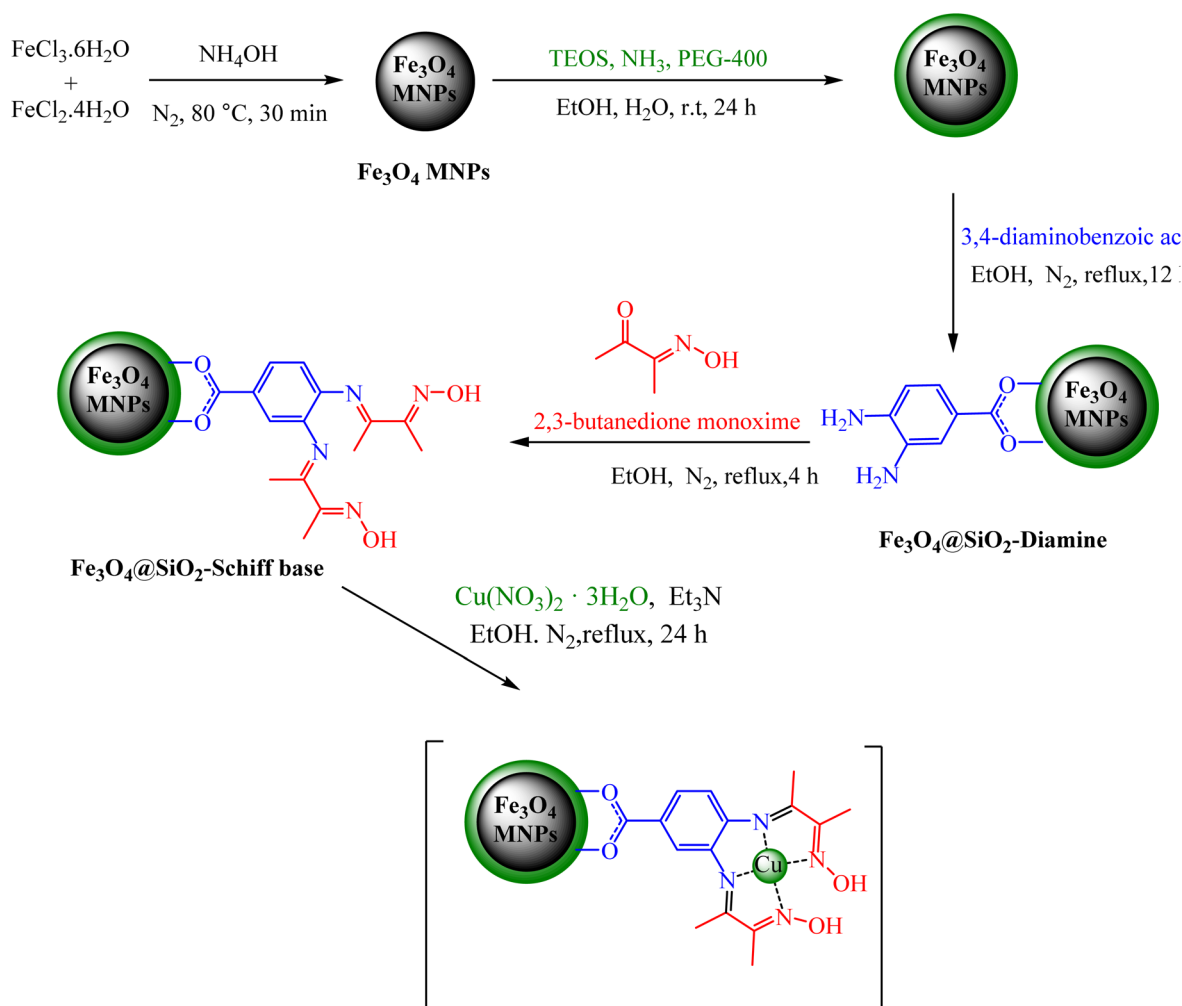
Scheme 1 Synthesis of [Fe$_3$O$_4$@SiO$_2$-Schiff base-Cu$^{(II)}$] complex.

collected, washed several times with ethanol and dried under vacuum. Afterwards, 1 g of Fe_3O_4@SiO_2-diamine was dispersed in ethanol for 30 minutes. Then, a 20 mL solution of 0.3 M 2,3-butanedione monoxime in ethanol was added dropwise to the reaction mixture, which was then refluxed for 4 hours under a N_2 atmosphere. The synthesized Fe_3O_4@SiO_2-Schiff base MNPs were accumulated, washed with ethanol and dried under vacuum. Next, 1 g of Fe_3O_4@SiO_2-Schiff base MNPs was dispersed in 100 mL of ethanol, and 3 drops of triethylamine and 25 mL of a 0.2 M ethanolic solution of $Cu(NO_3)_2 \cdot 3H_2O$ were added dropwise to the prepared suspension and refluxed for 24 hours under a N_2 atmosphere. Finally, the obtained [Fe_3O_4@-SiO_2-Schiff base-Cu[(II)]] complex was collected, purified through washing with water and dried under vacuum (Scheme 1).

2.2. General procedure to produce 2 pyrano[2,3-*c*]pyrazoles catalyzed *via* [Fe_3O_4@SiO_2-Schiff base-Cu[(II)]] complex

A mixture of ethyl acetoacetate (1 mmol) and hydrazine hydrate (1 mmol), [Fe_3O_4@SiO_2-Schiff base-Cu[(II)]] complex (12 mg), and 3 mL of water were mixed in a round-bottomed until 3-methyl-1*H*-pyrazol-5(4H)-one precipitate was formed. Following that, malononitrile (1 mmol), and aldehyde (1 mmol) were introduced into the flask and the reaction was agitated under reflux conditions. Once the reaction was deemed complete, which was monitored using thin-layer chromatography (TLC), a simple work-up procedure was performed. This involved using a magnetic field to separate the catalyst from the mixture (diluted with hot ethanol). The resulting crude products were then purified through recrystallization using a mixture of ethanol and diethyl ether and well-characterized by ^{1}H and ^{13}C NMR spectroscopy (ESI†).

3. Results and discussions

3.1. Catalyst characterization

FT-IR analysis was conducted to examine the formation of catalytic moieties on the surface. As depicted in Fig. 1, the FT-IR
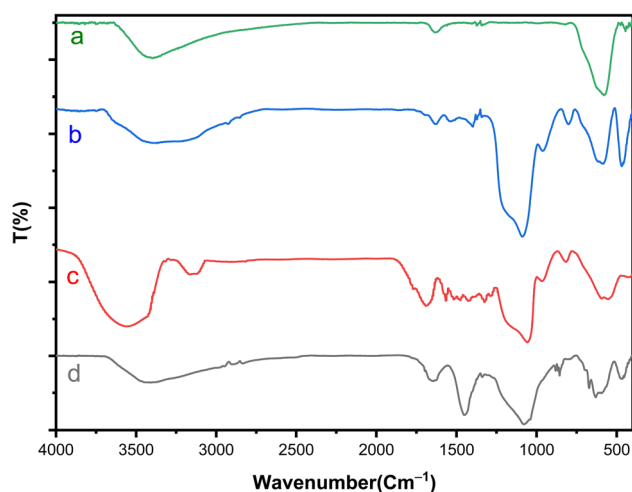
spectra of Fe_3O_4 and Fe_3O_4@SiO_2 align with previous reports regarding the characteristic features of these samples.[33] The peaks observed at 575 cm^{-1} and 619 cm^{-1} correspond to the mode of stretching vibrations in metal–oxygen bonds.[34] Furthermore, the faint peak at 810 cm^{-1} and the broad absorption peak ranging from 993 cm^{-1} to 1318 cm^{-1} can be ascribed to the stretching of Si–O–Si bonds.[35] The bands in the range of 2870 cm^{-1} to 2940 cm^{-1} and above 3000 cm^{-1} indicate the C–H stretching vibrations of aliphatic (methyl moieties) and aromatic C–H groups (present in the 3,4-diaminobenzoic acid) on the surface.[35] The peak appearing in the region of 3400 cm^{-1} is related to the N–H groups, which overlap with the O–H stretching vibrations. Additionally, the peaks in the 1200–1500 cm^{-1} range are related to C–N and C–O bonds. In the case of Fe_3O_4@SiO_2-Schiff base MNPs, the strong peak at 1627 cm^{-1} represents the stretching vibrations of C=N bonds and confirms the formation of imine groups. This indicates the attachment of the [Schiff base-Cu[(II)]] complex onto the nano-magnetic support.

The X-ray diffraction (XRD) analysis was conducted to examine the structural properties of the [Fe_3O_4@SiO_2-Schiff base-Cu[(II)]] complex (Fig. 2). The XRD pattern displayed the characteristic peaks of crystalline structure of Fe_3O_4 (JCPDS file no 19-0629) at $2\theta = 30.15°$, 35.65°, 43.33°, 53.89°, 57.31°, 62.89° and 74.33° that are related to planes (220), (311), (400), (422), (511), and (440), (533), respectively.[36] The results show that the post synthetic modification process did not change the crystalline structure of the final magnetic nanoparticles and it was remained intact. The presence of an amorphous SiO_2 layer can be confirmed by a broad peak at $2\theta = 24.29°$. The prepared catalyst exhibited some additional diffraction peaks at $2\theta = 24.29°$, 31.37°, 39.33° and 40.61 which could be due to the addition of [Schiff base-Cu[(II)]] complex on Fe_3O_4@SiO_2 surface.

The thermal stability of the [Fe_3O_4@SiO_2-Schiff base-Cu[(II)]] complex was investigated using TGA and DSC analysis (Fig. 3). The weight loss observed below 200 °C is due to the removal of organic solvents and moisture that were adsorbed.[37] Furthermore, a weight loss of approximately 23% was occurred at 200–470 °C, indicating the separation and breakdown of the Schiff

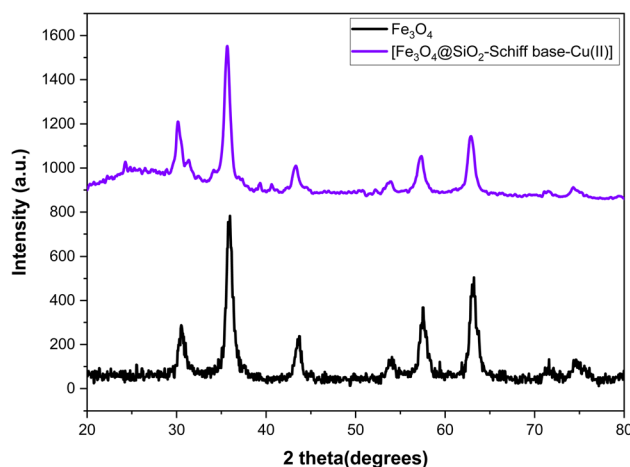**Fig. 1** FTIR spectrum of (a) Fe_3O_4, (b) Fe_3O_4@SiO_2, (c) Fe_3O_4@SiO_2-diamine and (d) [Fe_3O_4@SiO_2-Schiff base-Cu[(II)]] complex.

Fig. 2 XRD pattern of [Fe_3O_4@SiO_2-Schiff base-Cu[(II)]] complex.
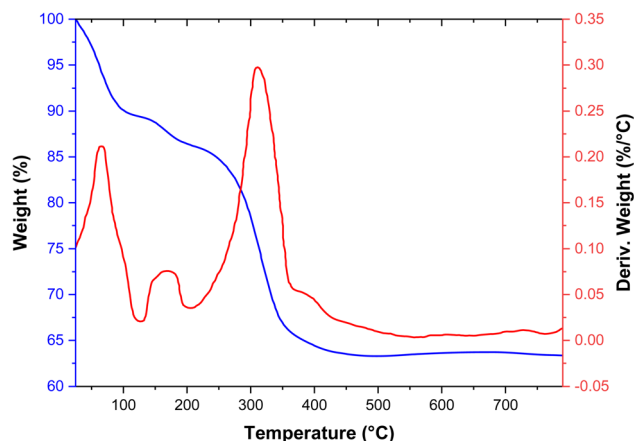
Fig. 3 The TGA–DSC curves of [Fe$_3$O$_4$@SiO$_2$-Schiff base-Cu$^{(II)}$] complex.

base organic groups from the nanocomposite surface through pyrolysis. This process was characterized by a noticeable endothermic peak in the DSC analysis. The nanocomposite demonstrated stability up to around 200 °C, thanks to the inherent thermal stability of the Schiff base design. Consequently, it can be easily employed in organic reactions and high-temperature conditions.

The elemental composition of the [Fe$_3$O$_4$@SiO$_2$-Schiff base-Cu$^{(II)}$] complex was examined through EDAX analysis (Fig. 4). This analysis confirmed the presence of distinct peaks corresponding to the Fe, Si, and O elements, which is consistent with the TGA results indicating that over 60% of the sample consists of inorganic materials, including the Fe$_3$O$_4$ support and SiO$_2$ shell surrounding its surface. Furthermore, the observation of peaks for C and N provides further confirmation of the synthesis of the Schiff base layer derived from the prepared ligand. Lastly, the presence of Cu in the sample confirms the successful bonding of electron-donor atoms to copper ions and

the formation of the desired catalyst. The results clearly demonstrate the successful preparation of the designed composite using the post-synthetic modification method.

Furthermore, the EDS mapping images clearly illustrate the even distribution of the [Schiff base-Cu$^{(II)}$] complex across the Fe$_3$O$_4$@SiO$_2$ surface (Fig. 5). The significant percentages of Fe, O, and Si elements indicate their prominent presence in the composite material. On the other hand, the presence of carbon and nitrogen elements can be attributed to the successful incorporation of the Schiff base ligand, which shows a homogeneous distribution within the composite structure. The close alignment between the distribution patterns of copper and nitrogen reinforces the evidence of effective coordination between N atoms and copper ions within the catalyst. Collectively, the EDS mapping analysis provides comprehensive visual evidence of the uniform distribution and elemental composition of the [Fe$_3$O$_4$@SiO$_2$-Schiff base-Cu$^{(II)}$] complex.

The morphology of the [Fe$_3$O$_4$@SiO$_2$-Schiff base-Cu$^{(II)}$] complex was examined using scanning electron microscopy (SEM). The SEM analysis, as depicted in Fig. 6, clearly demonstrated the uniform spherical shape of the resulting nanocomposite, characterized by a rough surface texture. A notable observation was made when comparing these particles to the uncoated Fe$_3$O$_4$ counterparts, revealing a noticeable increase in size. This size increment strongly indicates the presence of SiO$_2$ and [Schiff base-Cu$^{(II)}$] shells that envelop the Fe$_3$O$_4$ particles. Remarkably, the SEM analysis revealed no significant agglomeration in the sample, signifying the successful distribution and stability of the nanocomposite.

The structure and size of the [Fe$_3$O$_4$@SiO$_2$-Schiff base-Cu$^{(II)}$] complex were analyzed using HR-TEM (Fig. 7). The particles exhibited a nearly spherical shape and demonstrated a high level of crystallinity. Their sizes ranged from 25 to 32 nm. They were surrounded by an amorphous layer, which contributed to their irregular shape. This shape suggested that the Fe$_3$O$_4$ nanoparticles were well-dispersed, likely due to their small size
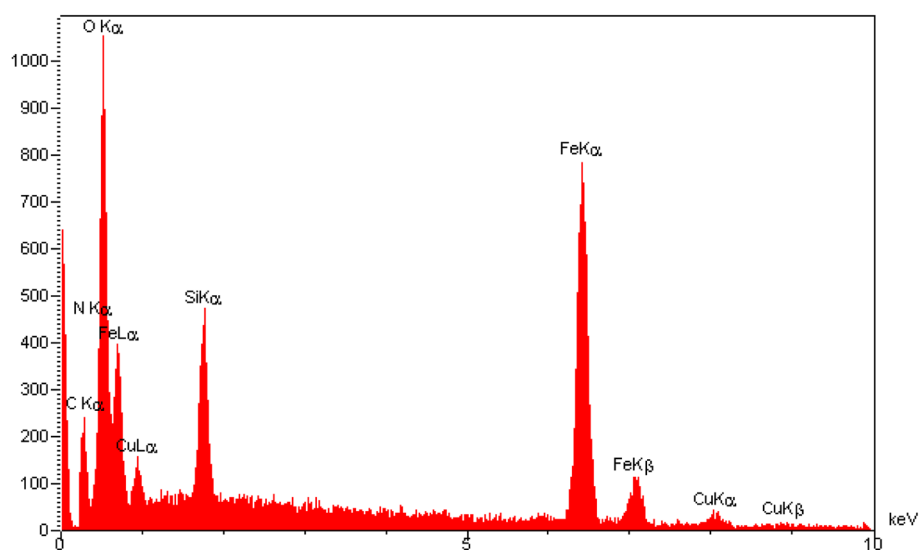

Fig. 4 The EDX analysis of the [Fe$_3$O$_4$@SiO$_2$-Schiff base-Cu$^{(II)}$] complex.
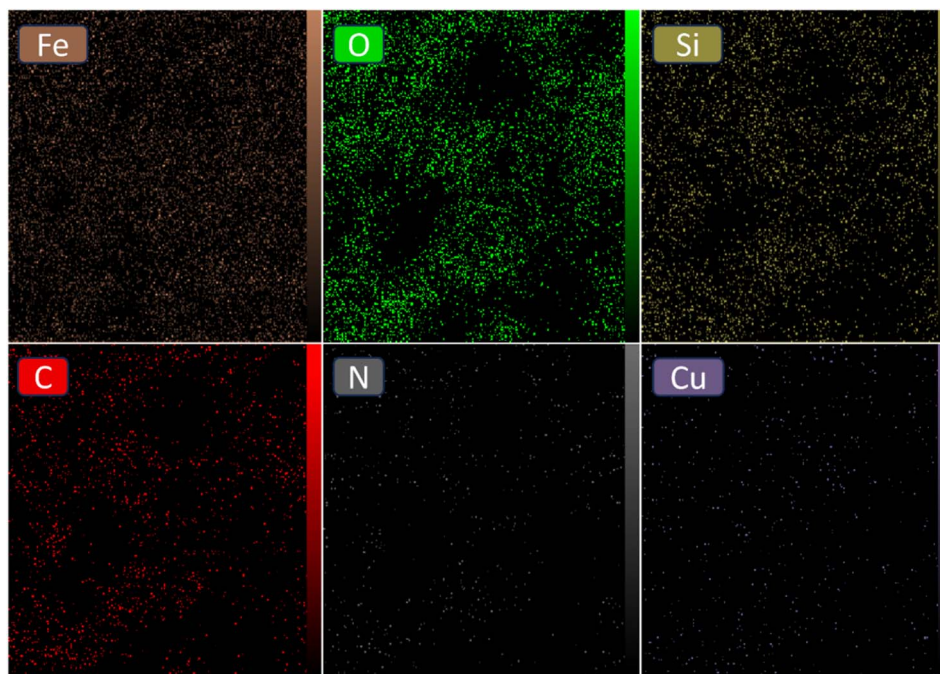
Fig. 5 The elemental mapping analysis of the [Fe$_3$O$_4$@SiO$_2$-Schiff base-Cu$^{(II)}$] complex.
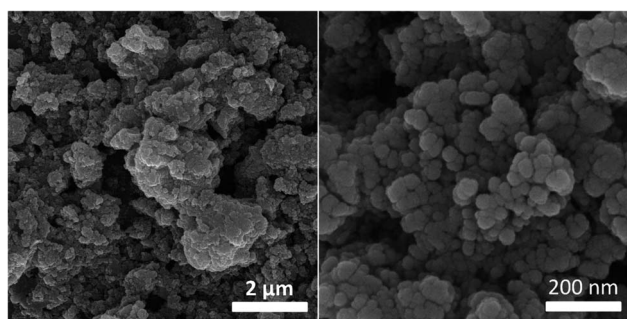
Fig. 6 SEM images of the [Fe$_3$O$_4$@SiO$_2$-Schiff base-Cu$^{(II)}$] complex.

and interaction with the grafted layers. In certain areas, some aggregation was observed, possibly attributed to the magnetic property of nanoparticles. These results confirm the successful formation of the desired complex on the surface of the modified magnetic nanoparticles.

Through BET analysis, the [Fe$_3$O$_4$@SiO$_2$-Schiff base-Cu$^{(II)}$] complex was examined to determine its isotherm type, surface area and pore characteristics (Fig. 8). The measured values were 27.2 nm, 39.59 m^2 g^{-1}, and 0.041 cm^3 g^{-1} for mean pore diameter, surface area, and total pore volume, respectively. The nanocomposite displayed a type IV isotherm and exhibited a mesoporous structure, evident from its average pore volume. Comparing these results with previous research, it can be inferred that the modification with [Schiff base-Cu$^{(II)}$] complex led to a reduction in the BET characteristics of Fe$_3$O$_4$@SiO$_2$. These surface characteristics of the [Fe$_3$O$_4$@SiO$_2$-Schiff base-Cu$^{(II)}$] complex provide ample reaction sites for direct interaction with organic reactants, resulting in an improved catalytic capacity.

The magnetic characteristics of the synthesized magnetic nanoparticles were evaluated using a vibration sample magnetometer (VSM). Fig. 9 provides a clear depiction of the saturation magnetization (M_s) values obtained for (a) Fe$_3$O$_4$, (b) Fe$_3$O$_4$@SiO$_2$, (c) Fe$_3$O$_4$@SiO$_2$-diamine, and (d) [Fe$_3$O$_4$@SiO$_2$-Schiff base-Cu$^{(II)}$] complex, which were determined as 74, 53, 33, and 24 emu g^{-1}, respectively. The introduction of an amorphous SiO$_2$ layer on the surface resulted in a notable decrease in the M_s value of Fe$_3$O$_4$ due to the non-magnetic nature silica. The difference in M_s values between Fe$_3$O$_4$@SiO$_2$ and Fe$_3$O$_4$@SiO$_2$-diamine indicated the bonding of a significant quantity of 3,4-diaminobenzoic acid groups to the surface of the Fe$_3$O$_4$ nanoparticles modified with silica. Moreover, the subsequent formation of organic functional groups (Schiff base) could diminish the surface moments of individual particles, leading to an overall reduction in magnetism. This decline in magnetic properties verifies the binding of iron nanoparticles to the [SiO$_2$-Schiff base-Cu$^{(II)}$] complex and validates its successful synthesis. Despite the lower M_s value of [Fe$_3$O$_4$@SiO$_2$-Schiff base-Cu$^{(II)}$] compared to pure Fe$_3$O$_4$, it remains adequate for effective magnetic separation, facilitating quicker removal from crude solutions.

3.2. Catalytic performance

We examined the performance of the magnetic [Fe$_3$O$_4$@SiO$_2$-Schiff base-Cu$^{(II)}$] complex as a catalyst in the one-pot reaction involving hydrazine hydrate, ethyl acetoacetate, benzaldehyde, and malononitrile, which serves as a model reaction for producing the desired pyrano[2,3-c]pyrazoles (Table 1). Initially, we investigated the model reaction under reflux conditions, using different green solvents such as water, alcohols, and
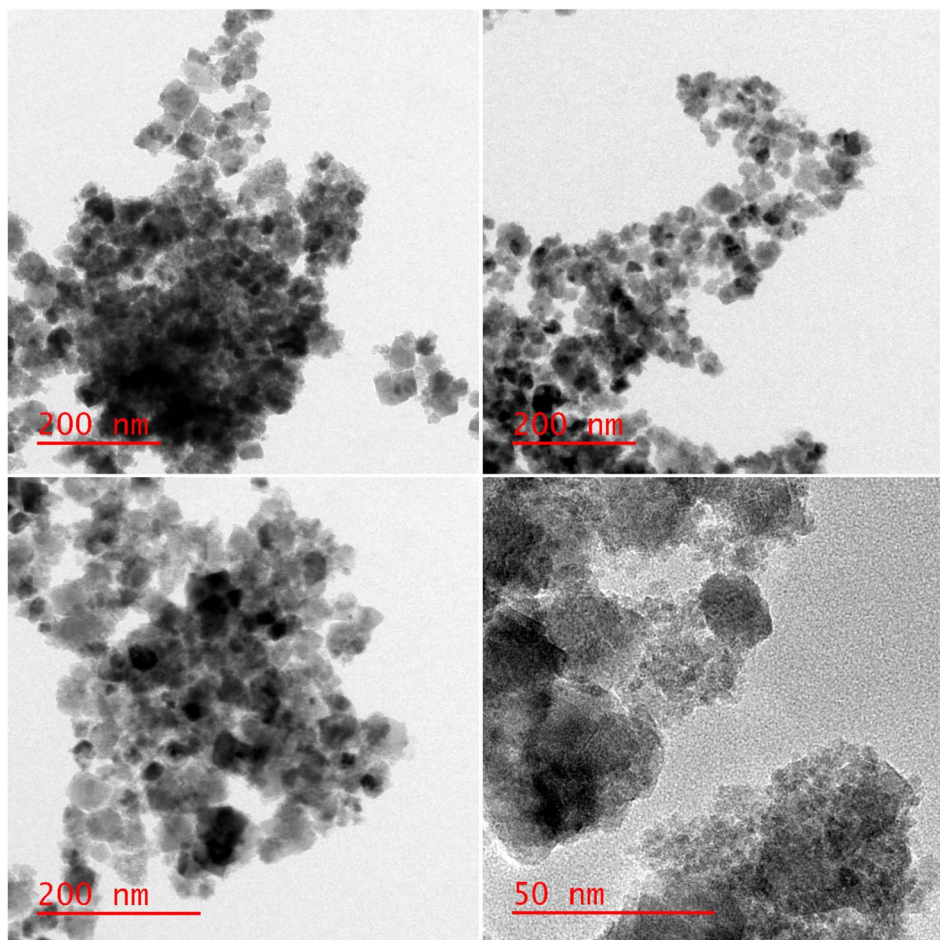
Fig. 7 TEM images of the [Fe_3O_4@SiO_2-Schiff base-$Cu^{(II)}$] complex.

solvent-free conditions. Fortunately, the results indicated that the highest yield was achieved when water was used as the solvent. Next, we examined the impact of catalyst loading and found that the best yield was obtained using 12 mg of the catalyst that was chosen as the minimum amount of the catalyst

Fig. 8 The N_2 adsorption–desorption isotherm of [Fe_3O_4@SiO_2-Schiff base-$Cu^{(II)}$] complex.

required for the transformation. Increasing the catalyst amount and extending the reaction duration did not enhance the reaction efficiency. Additionally, we studied the effect of temperature as another significant factor and observed a decrease in reaction efficiency when the temperature was lowered to room temperature. In the final optimization step, we compared the reaction under catalyst-free conditions and with catalyst intermediates to evaluate the desired Cu complex. The best outcome was obtained when the [Fe_3O_4@SiO_2-Schiff base-$Cu^{(II)}$] complex was used as the catalyst. Based on these findings, we determined that the optimal reaction conditions involved using 12 mg of [Fe_3O_4@SiO_2-Schiff base-$Cu^{(II)}$] complex in water under reflux conditions.

In next step, we explored the wide applicability and versatility of this method by utilizing the prescribed reaction conditions to examine a diverse range of aromatic and heteroaromatic aldehydes. This comprehensive set of aldehydes included various electron-donating and electron-withdrawing groups, such as halogens, nitro, methoxy, hydroxyl, and amino functionalities. The experimental results showcased exceptional yields of the desired pyrano[2,3-c]pyrazoles products, demonstrating the effectiveness of the approach (Table 2). Interestingly, we observed that the electron-withdrawing groups
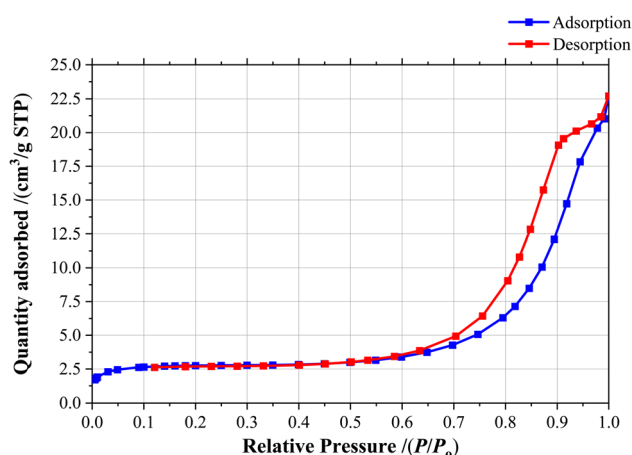
Fig. 9 The VSM analyses of (a) Fe_3O_4, (b) $Fe_3O_4@SiO_2$, (c) $Fe_3O_4@SiO_2$-diamine and (d) [$Fe_3O_4@SiO_2$-Schiff base-$Cu^{(II)}$] complex.

efficiency highlights the potential of this method for synthesizing pyrano[2,3-c]pyrazoles from a wide range of substrates, including those with complex and heterocyclic structures. Finally, an investigation into scaling up reactions was ultimately conducted using 15 mmol of benzaldehyde as the model substrate. This endeavor yielded the corresponding product in an excellent yield, effectively confirming the method's scalability and applicability.

Scheme 2 presents a proposed mechanism for [$Fe_3O_4@SiO_2$-Schiff base-$Cu^{(II)}$] complex catalyzed the synthesis of pyrano[2,3-c]pyrazoles.[48] The initial step involves the Cu-catalyzed cyclocondensation of a beta-keto ester and hydrazine hydrate, resulting in the formation of a five-membered N-heterocycle referred to as a pyrazalone intermediate. This pyrazalone intermediate demonstrates the presence of two resonance structures (II, III). Concurrently, Cu also facilitates the Knoevenagel condensation of aryl malononitrile and aldehydes. Subsequently, the pyrazalone intermediate engages in a Michael reaction with the β-aryl-α-cyanoacrylate compound generated from the Knoevenagel condensation. Subsequent to this, a Thorpe–Ziegler type cyclization takes place, result in the production of the corresponding pyrano[2,3-c]pyrazoles heterocycles.

Reusability and hot filtration tests. The reusability study of the [$Fe_3O_4@SiO_2$-Schiff base-$Cu^{(II)}$] complex was conducted on

significantly influenced both the reaction rate and yield, leading to the most favorable outcomes. This finding suggests that electronic and hindrance effects play a decisive role in reaction progress. Additionally, we successfully transformed heterocyclic carbaldehydes into the target products, achieving impressive yields within remarkably short reaction times. This remarkable

Table 1 Screening the reaction parameters for the synthesis of pyrano[2,3-c]pyrazoles under the catalysis of [$Fe_3O_4@SiO_2$-Schiff base-$Cu^{(II)}$]

Entry	Catalyst	Catalyst amount (mg)	Solvent	Temperature (°C)	Time (min)	Yield[a,b] (%)
1	[$Fe_3O_4@SiO_2$-Schiff base-$Cu^{(II)}$] complex	5	EtOH	Reflux	10	68
2	[$Fe_3O_4@SiO_2$-Schiff base-$Cu^{(II)}$] complex	5	MeOH	Reflux	10	65
3	[$Fe_3O_4@SiO_2$-Schiff base-$Cu^{(II)}$] complex	5	Water	Reflux	10	73
4	[$Fe_3O_4@SiO_2$-Schiff base-$Cu^{(II)}$] complex	5	PEG-400	100	10	70
5	[$Fe_3O_4@SiO_2$-Schiff base-$Cu^{(II)}$] complex	5	Solvent-free	100	10	58
6	[$Fe_3O_4@SiO_2$-Schiff base-$Cu^{(II)}$] complex	7	EtOH	Reflux	10	81
7	[$Fe_3O_4@SiO_2$-Schiff base-$Cu^{(II)}$] complex	9	EtOH	Reflux	10	93
8	[$Fe_3O_4@SiO_2$-Schiff base-$Cu^{(II)}$] complex	12	EtOH	Reflux	10	98
9	[$Fe_3O_4@SiO_2$-Schiff base-$Cu^{(II)}$] complex	14	EtOH	Reflux	10	98
10	[$Fe_3O_4@SiO_2$-Schiff base-$Cu^{(II)}$] complex	12	EtOH	Reflux	30	98
11	[$Fe_3O_4@SiO_2$-Schiff base-$Cu^{(II)}$] complex	12	EtOH	45	10	47
12	[$Fe_3O_4@SiO_2$-Schiff base-$Cu^{(II)}$] complex	12	EtOH	25	10	Trace
13	Catalyst free	—	EtOH	Reflux	12 h	Trace
14	Fe_3O_4	12	EtOH	Reflux	60	25
15	$Fe_3O_4@SiO_2$	12	EtOH	Reflux	60	21
16	$Fe_3O_4@SiO_2$-diamine	12	EtOH	Reflux	60	33
17	$Fe_3O_4@SiO_2$-Schiff base	12	EtOH	Reflux	60	47

[a] Conditions: ethyl acetoacetate (1 mmol), hydrazine hydrate (1 mmol), benzaldehyde (1 mmol), malononitrile (1 mmol) and (1 mmol), catalyst (mg) and solvent (3 mL). [b] Isolated yield.

Table 2 The synthesis of pyrano[2,3-c]pyrazoles catalyzed by [Fe₃O₄@SiO₂-Schiff base-Cu(II)] complex
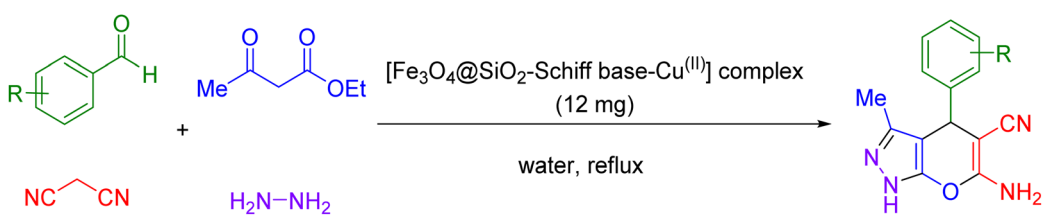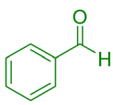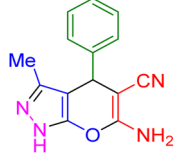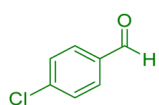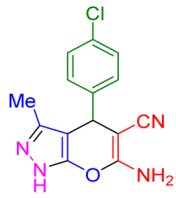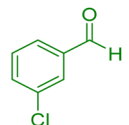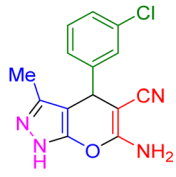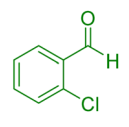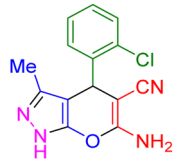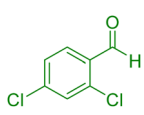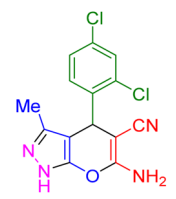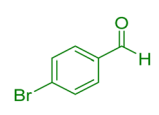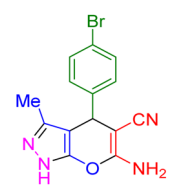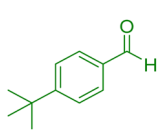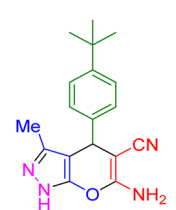
Entry	Aldehyde	Product	Time (min)	Yield[a,b] (%)	Melting point (°C)	
					Measured	Literature
1			10	98	243–245	243–245 (ref. 38)
2			12	98	234–236	234–236 (ref. 38)
3			15	96	230–231	229–230 (ref. 39)
4			20	94	238–240	237–240 (ref. 40)
5			30	93	195–197	196–198 (ref. 40)
6			15	97	181–183	180–182 (ref. 38)
7			25	96	221–222	221–222 (ref. 41)

Table 2 (*Contd.*)
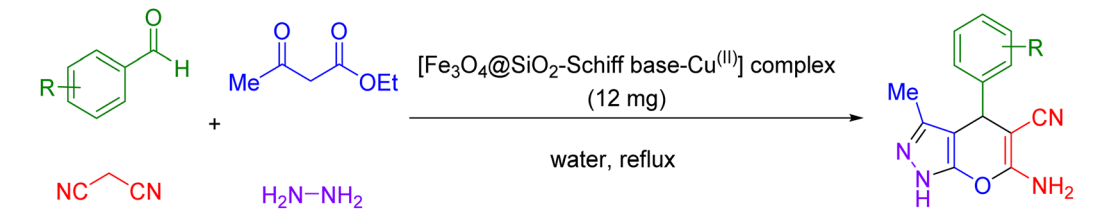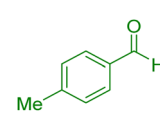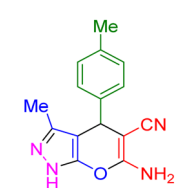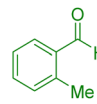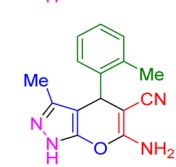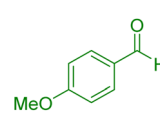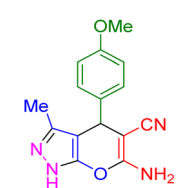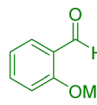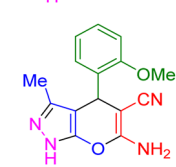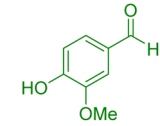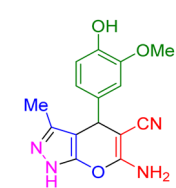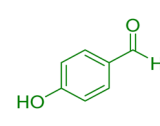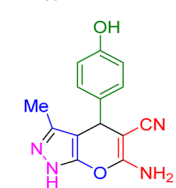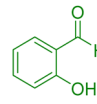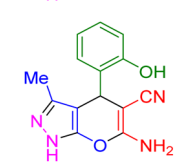
Entry	Aldehyde	Product	Time (min)	Yield[a,b] (%)	Melting point (°C)	
					Measured	Literature
8			20	95	207–209	207–209 (ref. 38)
9			35	94	172–174	172–174 (ref. 42)
10			30	91	209–211	209–211 (ref. 38)
11			45	88	246–248	246–248 (ref. 43)
12			55	90	235–237	235–237 (ref. 41)
13			35	92	221–223	222–224 (ref. 38)
14			70	87	209–211	209–211 (ref. 44)

Table 2 (*Contd.*)

Entry	Aldehyde	Product	Time (min)	Yield^{a,b} (%)	Melting point (°C)	
					Measured	Literature
15			70	87	227–228	227–228 (ref. 41)
16			20	87	182–184	182–183 (ref. 45)
17			75	88	218–220	218–219 (ref. 41)
18			10	99	250–251	250–251 (ref. 46)
19			45	90	229–231	228–230 (ref. 47)
20			75	89	214–215	215–216 (ref. 41)
21			65	86	223–224	222–224 (ref. 47)

^{a} Isolated yield. ^{b} Conditions: ethyl acetoacetate (1 mmol), hydrazine hydrate (1 mmol) arylaldehyde (1 mmol), malononitrile (1 mmol), [Fe$_3$O$_4$@SiO$_2$-Schiff base-Cu$^{(II)}$] (12 mg) in water solvent (3 mL) at reflux conditions.

the optimized catalytic model reaction. Following each reaction cycle, the insoluble catalyst was subjected to magnetic filtration and a thorough cleaning procedure involving hot water, ethanol, and acetone. This ensured the removal of any impurities or reaction byproducts before reusing the catalyst in subsequent cycles. Impressively, the catalyst exhibited
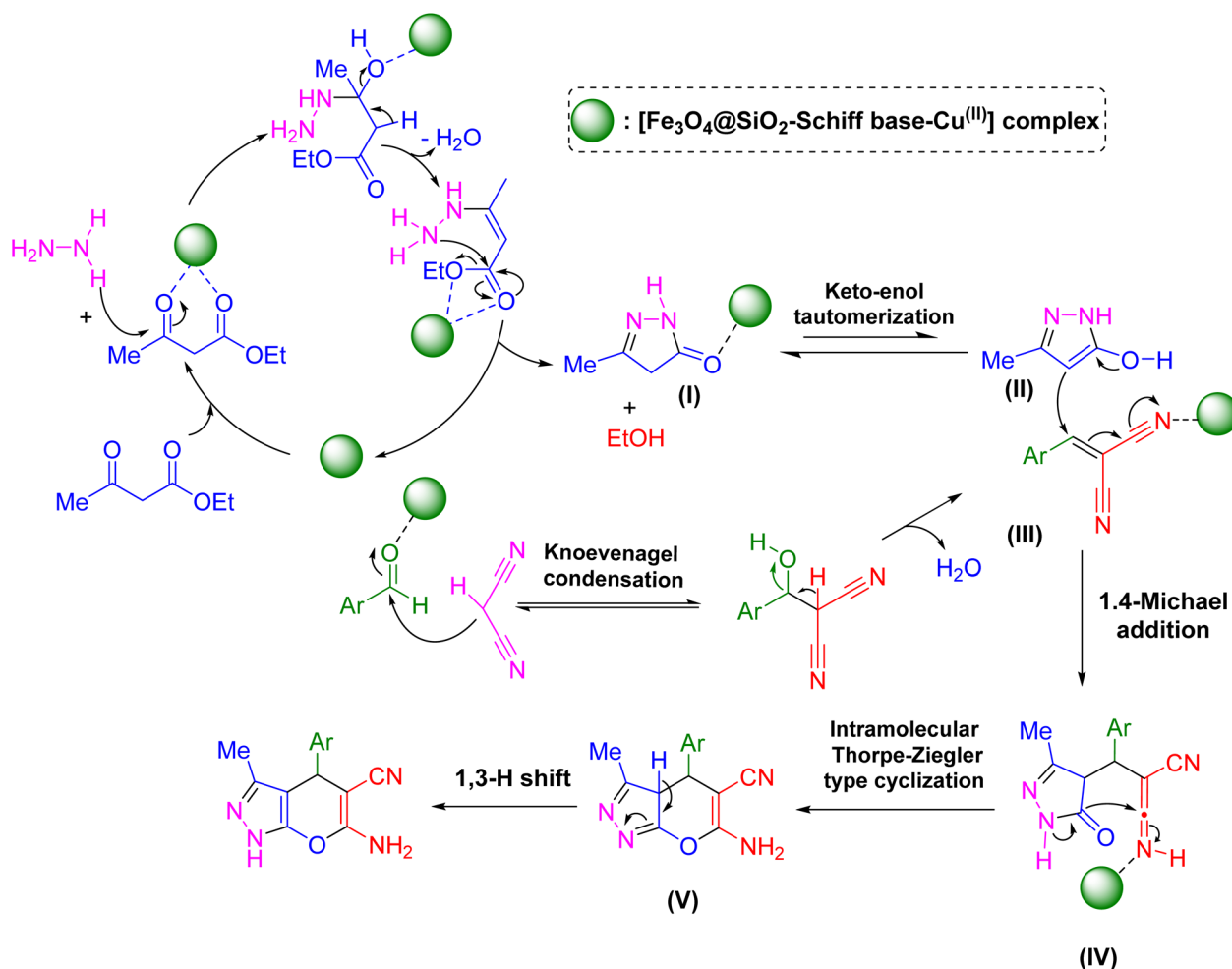
Scheme 2 Suggested reaction pathway for the synthesis of pyrano[2,3-*c*]pyrazoles facilitated by the catalytic properties of the [Fe$_3$O$_4$@SiO$_2$-Schiff base-Cu$^{(II)}$] complex.

outstanding stability throughout five cycles, maintaining its catalytic activity without any noticeable decrease in performance (Fig. 10). To further investigate its durability, a rigorous

Fig. 10 The reusability of [Fe$_3$O$_4$@SiO$_2$-Schiff base-Cu$^{(II)}$] complex.

hot filtration test was performed. At the midpoint of the reaction, the catalytic complex was removed while allowing the reaction to continue. Surprisingly, even with an extended reaction time, the product yield did not show a significant increase. Furthermore, the ICP-OES test revealed the absence of any notable quantity of copper metal within the filtered mixture. This observation strongly suggests that the catalytic complex possesses a heterogeneous nature, highlighting its ability to effectively facilitate the reaction without undergoing substantial structural changes or degradation.

Comparison. In Table 3, a comprehensive comparison was conducted to evaluate the efficiency of the synthesized [Fe$_3$O$_4$@SiO$_2$-Schiff base-Cu$^{(II)}$] complex in relation to recently studied catalysts for pyrano[2,3-*c*]pyrazoles synthesis. The results unequivocally demonstrate that our study achieved a significantly higher yield compared to other catalysts. Moreover, our suggested reaction conditions not only prioritize safety but also maintain one of the highest recorded yields for this specific reaction. These remarkable advantages solidify the developed method as an exceptionally efficient catalytic system, making it highly suitable for environmental cleanup and
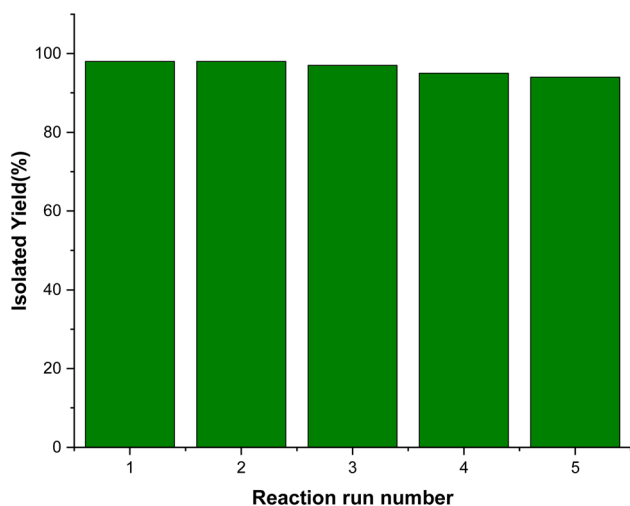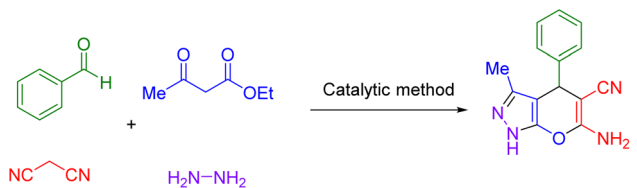
Table 3 Comparison of the catalytic performance of [Fe$_3$O$_4$@SiO$_2$-Schiff base-Cu$^{(II)}$] complex in synthesis of pyrano[2,3-*c*]pyrazoles model reaction[a]

Entry	Catalyst	Time (min)	Yield (%)	Ref[a]
1	Mg–Al hydrotalcite	60	87	49
2	ZnO NPs	60	94	50
3	Thiamine hydrochloride	15	91	51
4	ZnS NPs	8	92	52
5	Ru^{III}@CMC/Fe$_3$O$_4$	30	93	39
6	Fe$_3$O$_4$@SiO$_2$/Si(OEt)(CH$_2$)$_3$NH/CC/EDA/Cu(OAc)$_2$	6	86	53
7	Fe$_3$O$_4$@SiO$_2$/Si(OEt)(CH$_2$)$_3$@melamine@TC@Cu(OAc)$_2$	7	92	54
8	[Fe$_3$O$_4$@SiO$_2$-Schiff base-Cu$^{(II)}$] complex	10	98	This work

[a] Isolated yield.

positioning it as a highly promising candidate for diverse industrial applications.

Conclusion

In conclusion, our study successfully synthesized a heterogeneous Schiff base complex of copper-modified magnetic Fe$_3$O$_4$ catalyst, which was thoroughly characterized. This complex proved to be highly efficient in catalyzing the synthesis of pyrano[2,3-*c*]pyrazole derivatives. The structural and morphological analysis provided confirmation of the successful synthesis of the magnetic [Fe$_3$O$_4$@SiO$_2$-Schiff base-Cu$^{(II)}$] complex. Through the direct cyclization of *in situ* generated pyrazalone and substituted β-aryl-α-cyanoacrylate intermediates, we were able to synthesize a series of pyrazole compounds fused with 4-substituted pyran derivatives. This study offered notable advantages, including the simplicity of the experimental procedures and the ease of recovering the [Fe$_3$O$_4$@SiO$_2$-Schiff base-Cu$^{(II)}$] complex through magnetic separation, which could be repeated for at least five cycles. These findings contribute to the development of efficient and practical catalytic systems for producing derivatives of pyrano[2,3-*c*]pyrazole. Further research in this area may explore the potential applications of these compounds in various fields such as pharmaceuticals, agrochemicals, and materials science.

Ethical statement

There are no human or animal studies in this work.

Data availability

All data generated or analysed during this study are included in this published article and its ESI† files.

Author contributions

Rehab Tahseen alhayo and Ghufran Sh. Jassim: writing -original draft, review/editing, synthesis, characterization, and analysis of catalyst. Hasanain Amer Naji: catalysis studies and analysis. A. H. Shather: software and review/editing. Israa Habeeb Naser: analysis, acquiring research funding. Luay Ali Khaleel: analysis, review/editing, acquiring research funding. Haider Abdulkareem Almashhadani: conceptualization, analysis, review draft, acquiring research funding and supervision.

Conflicts of interest

The authors declare no competing interests.

References

1 H. T. Nguyen, M. N. H. Truong, T. Van Le, N. T. Vo, H. D. Nguyen and P. H. Tran, *ACS Omega*, 2022, **7**, 17432–17443.

2 S. Sikandar and A. F. Zahoor, *J. Heterocycl. Chem.*, 2021, **58**, 685–705.

3 T. E. Ali, D. A. Bakhotmah and M. A. Assiri, *Synth. Commun.*, 2020, **50**, 3314–3325.

4 F. Ghorbanipour, S. M. Nezhad, S. A. Pourmousavi, E. N. Zare and G. Heidari, *Inorg. Chem. Commun.*, 2023, **147**, 110271.

5 S. A. El-Assaly, A. E. H. A. Ismail, H. A. Bary and M. G. Abouelenein, *Curr. Chem. Lett.*, 2021, **10**, 309–328.

6 M. E. A. Zaki, H. A. Soliman, O. A. Hiekal and A. E. Rashad, *Z. Naturforsch. Sect. C J. Biosci.*, 2006, **61**, 1–5.

7 M. Mohammadi, A. Ghorbani-Choghamarani and N. Hussain-Khil, *J. Phys. Chem. Solids*, 2023, **177**, 111300.

8 R. Eivazzadeh-Keihan, R. Taheri-Ledari, N. Khosropour, S. Dalvand, A. Maleki, S. M. Mousavi-Khoshdel and H. Sohrabi, *Colloids Surf., A*, 2020, **587**, 124335.

9 K. Pradhan, S. Paul and A. R. Das, *Catal. Sci. Technol.*, 2014, **4**, 822.

10 M. A. Ghasemzadeh, B. Mirhosseini-Eshkevari and J. Dadashi, *J. Mol. Struct.*, 2022, **1261**, 132843.

11 M. A. Ghasemzadeh, B. Mirhosseini-Eshkevari and J. Dadashi, *Sci. Rep.*, 2023, **13**, 9089.

12 Y. Guo, S. A. Delbari, A. Sabahi Namini, Q. Van Le, J. Y. Park, D. Kim, R. S. Varma, H. W. Jang, A. T. Raissi, M. Shokouhimehr and C. Li, *Mol. Catal.*, 2023, **547**, 113362.

13 L. Zare Fekri, M. Nateghi-Sabet and M. Nikpassand, *Org. Prep. Proced. Int.*, 2022, **54**, 449–456.

14 F. Casti, F. Basoccu, R. Mocci, L. De Luca, A. Porcheddu and F. Cuccu, *Molecules*, 2022, **27**, 1988.

15 M. Nikpassand, L. Z. Fekri and A. Pourahmad, *Lett. Org. Chem.*, 2020, **17**, 360–365.

16 P. Shakib, M. G. Dekamin, E. Valiey, S. Karami and M. Dohendou, *Sci. Rep.*, 2023, **13**, 8016.

17 A. Simon and S. Mathai, *J. Organomet. Chem.*, 2023, **996**, 122768.

18 M. Nikpassand, A. Keyhani, L. Z. Fekri and R. S. Varma, *J. Mol. Struct.*, 2022, **1251**, 132065.

19 M. Liu, Y. Ye, J. Ye, T. Gao, D. Wang, G. Chen and Z. Song, *Magnetochemistry*, 2023, **9**, 110.

20 M. Torabi, L. Z. Fekri and M. Nikpassand, *J. Mol. Struct.*, 2022, **1250**, 131761.

21 W. Xie and J. Li, *Renewable Sustainable Energy Rev.*, 2023, **171**, 113017.

22 M. Sajjadi, M. Nasrollahzadeh, H. Ghafuri, T. Baran, Y. Orooji, N. Y. Baran and M. Shokouhimehr, *Int. J. Biol. Macromol.*, 2022, **209**, 1573–1585.

23 R. Malav and S. Ray, *Inorg. Chim. Acta*, 2023, **551**, 121478.

24 D. I. Ugwu and J. Conradie, *Inorg. Chim. Acta*, 2023, **553**, 121518.

25 H. Keypour, J. Kouhdareh, S. Alavinia, K. Rabiei, M. Mohammadi, A. Maryamabadi and S. Babaei, *J. Organomet. Chem.*, 2023, **989**, 122646.

26 K. Rabiei, Z. Mohammadkhani, H. Keypour and J. Kouhdareh, *RSC Adv.*, 2023, **13**, 8114–8129.

27 V. D. Manvatkar, R. Y. Patle, P. H. Meshram and R. S. Dongre, *Chem. Pap.*, 2023, **77**(10), 5641–5662.

28 A. Tombesi and C. Pettinari, *Inorganics*, 2021, **9**, 81.

29 M. K. Patil, V. H. Masand and A. K. Maldhure, *Curr. Nanosci.*, 2020, **17**, 634–645.

30 H. Ahmad and M. K. Hossain, *Mater. Adv.*, 2022, **3**, 859–887.

31 C. Liu, *Synth. Commun.*, 2021, **51**, 2237–2264.

32 M. Kazemnejadi, S. A. Alavi G., Z. Rezazadeh, M. A. Nasseri, A. Allahresani and M. Esmaeilpour, *Appl. Organomet. Chem.*, 2020, **34**, e5388.

33 X. Tan, P. Sudarsanam, J. Tan, A. Wang, H. Zhang, H. Li and S. Yang, *J. Environ. Chem. Eng.*, 2021, **9**, 104719.

34 F. Ghobakhloo, D. Azarifar, M. Mohammadi and M. Ghaemi, *Appl. Organomet. Chem.*, 2022, **36**, e6823.

35 S. Ghorbani, D. Habibi, S. Heydari, M. Mohammadi and M. Ariannezhad, *Environ. Sci. Pollut. Res.*, 2022, **30**, 32762–32775.

36 R. H. Althomali, M. K. Abbood, F. M. A. Altalbawy, E. A. M. Saleh, S. S. Abdullaev, A. jaber Ibrahim, S. A. Ansari and R. M. Romero-Parra, *J. Mol. Struct.*, 2023, **1290**, 135911.

37 F. Ghobakhloo, D. Azarifar and M. Mohammadi, *J. Phys. Chem. Solids*, 2023, **175**, 111222.

38 F. Mohamadpour, *J. Chem. Sci.*, 2020, **132**, 72.

39 Y. Chen, Z. Zhang, W. Jiang, M. Zhang and Y. Li, *Mol. Diversity*, 2019, **23**, 421–442.

40 F. Hassanzadeh-Afruzi, H. Dogari, F. Esmailzadeh and A. Maleki, *Appl. Organomet. Chem.*, 2021, **35**, e6363.

41 H. T. Nguyen, T. Van Le and P. H. Tran, *J. Environ. Chem. Eng.*, 2021, **9**, 105228.

42 N. Hosseini Mohtasham and M. Gholizadeh, *Res. Chem. Intermed.*, 2020, **46**, 3037–3066.

43 M. M. Heravi, R. Malakooti, K. Kafshdarzadeh, Z. Amiri, V. Zadsirjan and H. Atashin, *Res. Chem. Intermed.*, 2022, **48**, 203–234.

44 K. G. Patel, N. M. Misra, R. H. Vekariya and R. R. Shettigar, *Res. Chem. Intermed.*, 2018, **44**, 289–304.

45 A. B. Atar, J. T. Kim, K. T. Lim and Y. T. Jeong, *Synth. Commun.*, 2014, **44**, 2679–2691.

46 R. Kumari, A. Varghese, L. George and K. B. Akshaya, *J. Mol. Liq.*, 2016, **222**, 828–835.

47 M. Bakherad, A. Keivanloo, M. Gholizadeh, R. Doosti and M. Javanmardi, *Res. Chem. Intermed.*, 2017, **43**, 1013–1029.

48 B. Halder, H. S. Maity, F. Banerjee, A. B. Kachave and A. Nag, *Polycyclic Aromat. Compd.*, 2022, **42**, 3302–3317.

49 S. W. Kshirsagar, N. R. Patil and S. D. Samant, *Synth. Commun.*, 2011, **41**, 1320–1325.

50 S. U. Tekale, S. S. Kauthale, K. M. Jadhav and R. P. Pawar, *J. Chem.*, 2013, **2013**, 1–8.

51 M. D. Nikam, P. S. Mahajan, A. V. Chate, S. K. Dabhade and C. H. Gill, *J. Chil. Chem. Soc.*, 2015, **60**, 2847–2850.

52 A. V. Borhade and B. K. Uphade, *J. Iran. Chem. Soc.*, 2015, **12**, 1107–1113.

53 A. Ghanbarpour, A. Khazaei, A. R. Moosavi-Zare, T. Akbarpour, M. Mohammadi and N. Sarmasti, *Polycycl. Aromat. Compd.*, 2023, **43**, 3192–3215.

54 M. Soleimani, T. Akbarpour and A. Khazaei, *Polycycl. Aromat. Compd.*, 2023, 1–27.